Supplementary Information

Efficient Descriptors for the Design of High-Performance Zr-Doped Ni-Based Catalysts for the Hydrogenation of 1,4-Butynediol to 1,4-Butanediol

Zhou Chen[a], Xueqing Hai[a], Xiangdong Geng[b], Hu shi[c], Yongxiang Zhao[a], Changzhen Wang *[a]

a. *Engineering Research Center of Ministry of Education for Fine Chemicals, Shanxi University, Taiyuan 030006, Shanxi Province, PR China.*
   * Corresponding author: czwang@sxu.edu.cn

b. *School of Materials Science and Engineering, Zhengzhou University, Zhengzhou, 450001, PR China.*

c. *School of Chemistry and Chemical Engineering, Institute of Molecular Science, Shanxi University, Taiyuan 030006, PR China.*

Content includes: Computational Section, 16 Figures and 2 Tables.

Fig. S1. The relationship between BYD adsorption and (a) Ni (111) and (b) Zr1-Ni (111). The corresponding structural diagrams are shown in (c) Ni (111) and (d) Zr1-Ni (111).

Fig. S2. The optimized possible catalyst's structure of (a1-a3) Zr5–Ni (111) surface and (b1-b5) Zr9–Ni (111) surface.

Fig. S3. Calculated Bader charge of (a) Zr1-Ni (111) (b) Zr5-Ni (111) and (c) Zr9-Ni (111) catalyst surface. Blue and red represent the electron accumulation and depletion region, respectively.

Fig. S4. Density of state (DOS) of Ni (111) (a), Zr1–Ni (111) (b), Zr5–Ni (111) (c) and Zr9–Ni (111) (d).

Fig. S5. The side and top perspectives of the most stable adsorption energies and binding sites of the H atom on (a) Ni (111) surface.

Fig. S6. The side and top perspectives of the most stable adsorption energies and binding sites of the H atom on (a) Zr1-Ni (111) surface.

Fig. S7. The side and top perspectives of the most stable adsorption energies and binding sites of the H atom on Zr5-Ni (111) surface.

Fig. S8. The side and top perspectives of the most stable adsorption energies and binding sites of the H atom on Zr9-Ni (111) surface.

Fig. S9. Correlation between the (a-c) Δd of Zrx-Ni (111) surface and different intermediates Ads energy (adsorption energy).

Fig. S10. Illustration of the whole energy diagram depicting the BYD hydrogenation process step on different catalysts.

Fig. S11. Geometries of the transition states over the Ni (111). The numbers represent C-C triple bond and Zr-O bond lengths; bond lengths are in Å.

Fig. S12. Geometries of the transition states over the Zr1-Ni (111). The numbers represent C-C triple bond and Zr-O bond lengths; bond lengths are in Å.

Fig. S13. Geometries of the transition states over the Zr5Ni (111). The numbers represent C-C triple bond and Zr-O bond lengths; bond lengths are in Å.

Fig. S14. The spin-down ICOHPs of C=C in cis-BED adsorbed on (a1) Ni (111), (b1) Zr1-Ni (111), (c1) Zr5-Ni (111), and (d1) Zr9-Ni (111). (a2-d2) is the PDOS of the absorbed cis-BED in Ni (111) or heterogeneous system.

Fig. S15. Calculated Bader charge of cis-BED adsorption on Zr9-Ni (111) catalyst surface. Blue and red represent the electron accumulation and depletion region, respectively.

Fig. S16. Charge density difference for cis-BED adsorption on Zr9-Ni (111). Cyan and yellow mean electron depletion and accumulation, respectively. The value of the isosurface is 0.02 eBohr^{-3}

Table S1 Energy of Optimized structure of doping system.

Table S2 The d-band center of different site. The unit is eV.

Computational Section

Theoretical method: The investigation of the electronic structure and potential energy surface (PES) of spin-polarized Ni-Zr surface systems was carried out using the Vienna Ab initio Simulation Package (VASP)[1, 2], which relied on density functional theory (DFT). To model the interactions between electrons and ions, the projector augmented wave (PAW)[3, 4] pseudopotential method was utilized. The description of the exchange-correlation functional was made using the Perdew–Burke–Ernzerhof (PBE)[5] form of the generalized gradient approximation (GGA). For the calculations, a plane wave cutoff energy of 400 eV was chosen, accompanied by Monkhorst-Pack[6] k-point sampling configurations of $10 \times 10 \times 10$ for bulk structures and $3 \times 3 \times 1$ for surface structures. Energy minimization of the ground state was performed until the criteria for electron self-consistency reached 1×10^{-6} eV, ensuring that the Hellmann-Feynman forces acting on each atom were less than 0.02 eV/Å. Geometric relaxation was achieved through a conjugate gradient algorithm, while Gaussian broadening was applied for wave function smoothing. The density of states (DOS) was computed employing the tetrahedral method with Blöchl correction, which provides fractional occupation values of the electron orbitals. Additionally, van der Waals forces were incorporated using the D3[7] empirical correction scheme. To prevent artificial interactions between the top and bottom atomic layers of the surface slab, a vacuum layer with a thickness of 15 Å was employed. (Fig. S1) The atoms in the bottom two layers were fixed at their equilibrium bulk positions, while the atoms in the upper two layers and the adsorbates were allowed to relax. All gas-phase molecules were optimized using a $20 \times 20 \times 20$ grid under a $6 \times 6 \times 6$ k-point sampling.

Density of states (DOS) and Crystal Orbital Hamilton Population (COHP) calculations: The density of states (DOS) served to characterize the electronic state distribution. In this context, the projected density of states (PDOS) highlights the contributions of various atomic orbitals to the overall DOS. Furthermore, quantifying the strength of chemical bonds was accomplished through Crystal Orbital Hamilton Population (COHP) calculations, executed via the Lobster program package[8]. COHP values were integrated up to the Fermi energy level (ICOHP) to specifically evaluate the strength of chemical bonds. Usually, the more negative the ICOHP, the stronger the bond. The d-band center gap of spin state (Δd) can be defined as

$$\Delta d = |\varepsilon_{up} - \varepsilon_{dw}| = \left| \frac{\int\limits_{-\infty}^{+\infty} n_{up}(\varepsilon)\varepsilon d\varepsilon}{\int\limits_{-\infty}^{+\infty} n_{up}(\varepsilon) d\varepsilon} - \frac{\int\limits_{-\infty}^{+\infty} n_{dw}(\varepsilon)\varepsilon d\varepsilon}{\int\limits_{-\infty}^{+\infty} n_{dw}(\varepsilon) d\varepsilon} \right| \quad (1)$$

where ε_{UP} is the d-band center of the Ni 3d spin-up projected density of states. And ε_{DW} is the d-band center of the Ni 3d spin-down projected density of states.

Adsorption energy, differential charge density and bader charge calculations: Adsorption energy, indicating the energy release associated with the adhesion of atoms or molecules to a surface during the adsorption process, quantifies the difficulty level of this adhesion. It can be expressed as the energy difference between the initial and final states of adsorption. The formula used for calculating the adsorption energy of different molecules on the Ni-Zr surface is:

$$E_{ads} = E_{surface + molecule} - E_{surface} - E_{molecule} \quad (2)$$

In this equation, $E_{surface + molecule}$ is the total energy of the surface with an adsorbed molecule. $E_{surface}$ is the energy of the pure surface slab and $E_{molecule}$ is the energy of a different molecule in a vacuum. Additionally, defining the differential charge density involves calculating the difference between the total charge density of the entire system and the sum of the charge densities of its separate components. This analysis is aimed at understanding charge transfer characteristics and the directionality of bonding polarization during bond formation and electronic coupling processes. This allows for a clearer interpretation of electron dynamics that occur during interactions among constituents, as well as the changes in electron density occurring throughout molecular formation, defined as Eq. (2):

$$\Delta\rho = \rho_{AB} - \rho_A - \rho_B \quad (3)$$

In this expression, ρ_{AB} is the charge density of AB segment, ρ_A is the charge density of A segment, ρ_B is the charge density of B segment. It is important to maintain a consistent model size for each charge density calculation. Bader charge analysis was performed using the Henkelman code via a near-grid algorithm with edge refinement.

Transition state (TS) calculations: Transition state (TS) searches were performed using both the climbing image Nudge Elastic Band (CI-NEB)[9] method and Henkelman's Dimer method[10, 11]. For the CI-NEB steps, electronic and geometric convergence criteria were set at 10^{-7} eV and 0.5 Å, respectively, while dimer calculations required convergence criteria of 10^{-7} eV and 0.05 Å.

Verification of all transition states confirmed the presence of only one imaginary frequency associated with the reaction pathway.
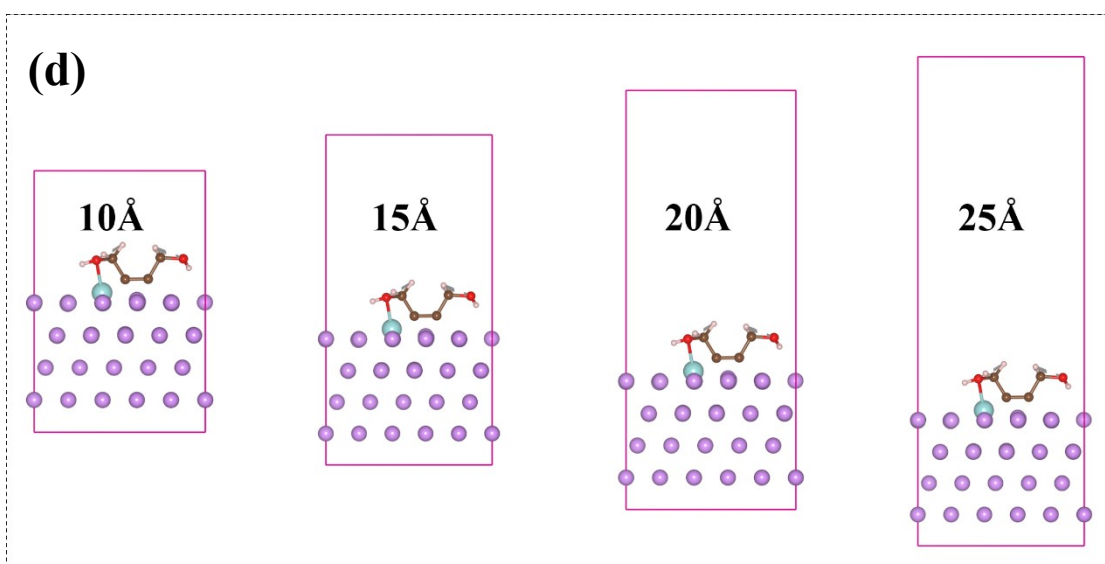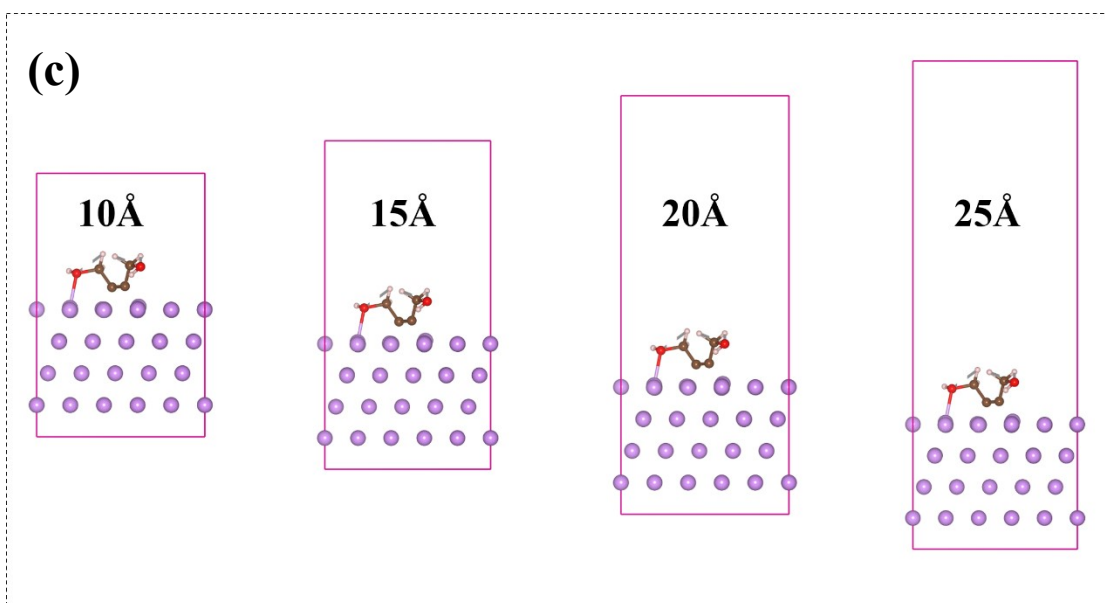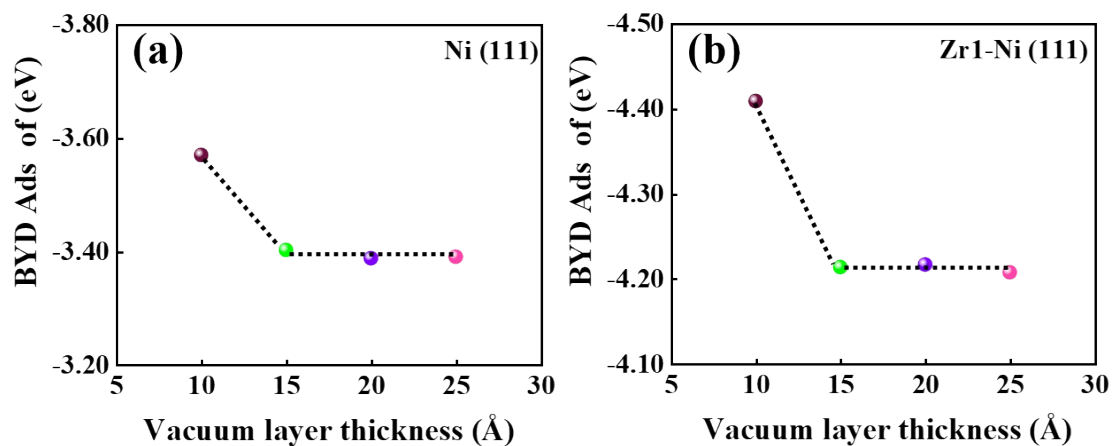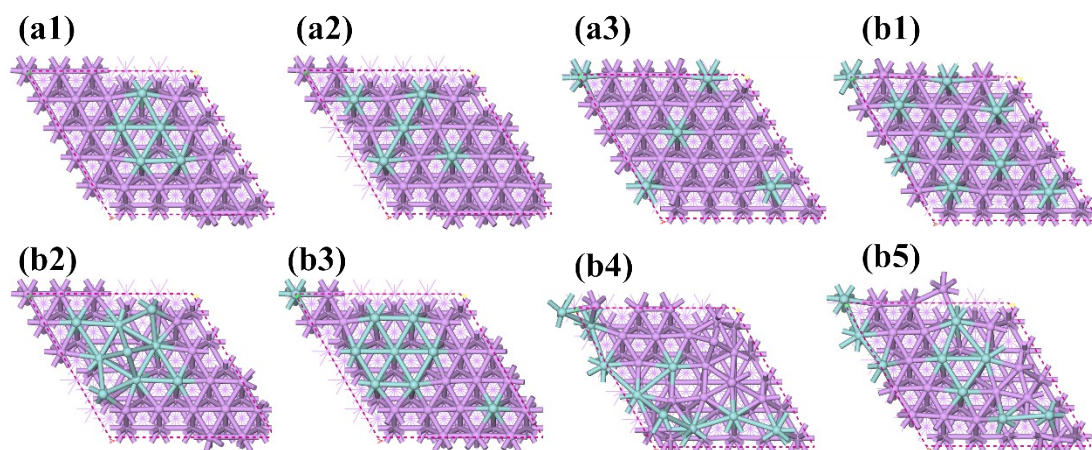
Fig. S1. The relationship between BYD adsorption and (a) Ni (111) and (b) Zr1-Ni (111). The corresponding structural diagrams are shown in (c) Ni (111) and (d) Zr1-Ni (111).
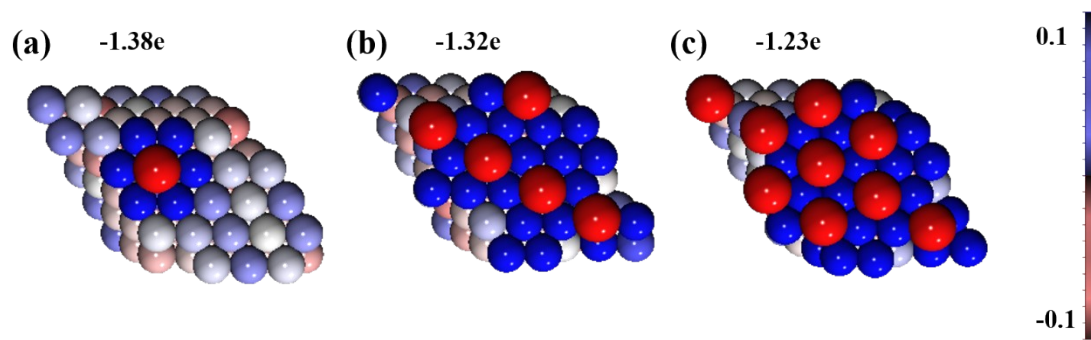
Noting: As shown in Fig. S1, we evaluated the selection of the vacuum layer about the 5×5×4

supercell of Ni (111). Fig. S1a and c demonstrated that the adsorption energy of BYD stabilized at approximately -3.40 eV when the vacuum layer was set to 15 Å. Notably, for the 5×5×4 supercell of Zr1-Ni (111), the model also exhibited similar results, with BYD's adsorption energy stabilizing at -4.20 eV. Based on these tests, we adopted a vacuum layer of 15 Å for subsequent calculations.
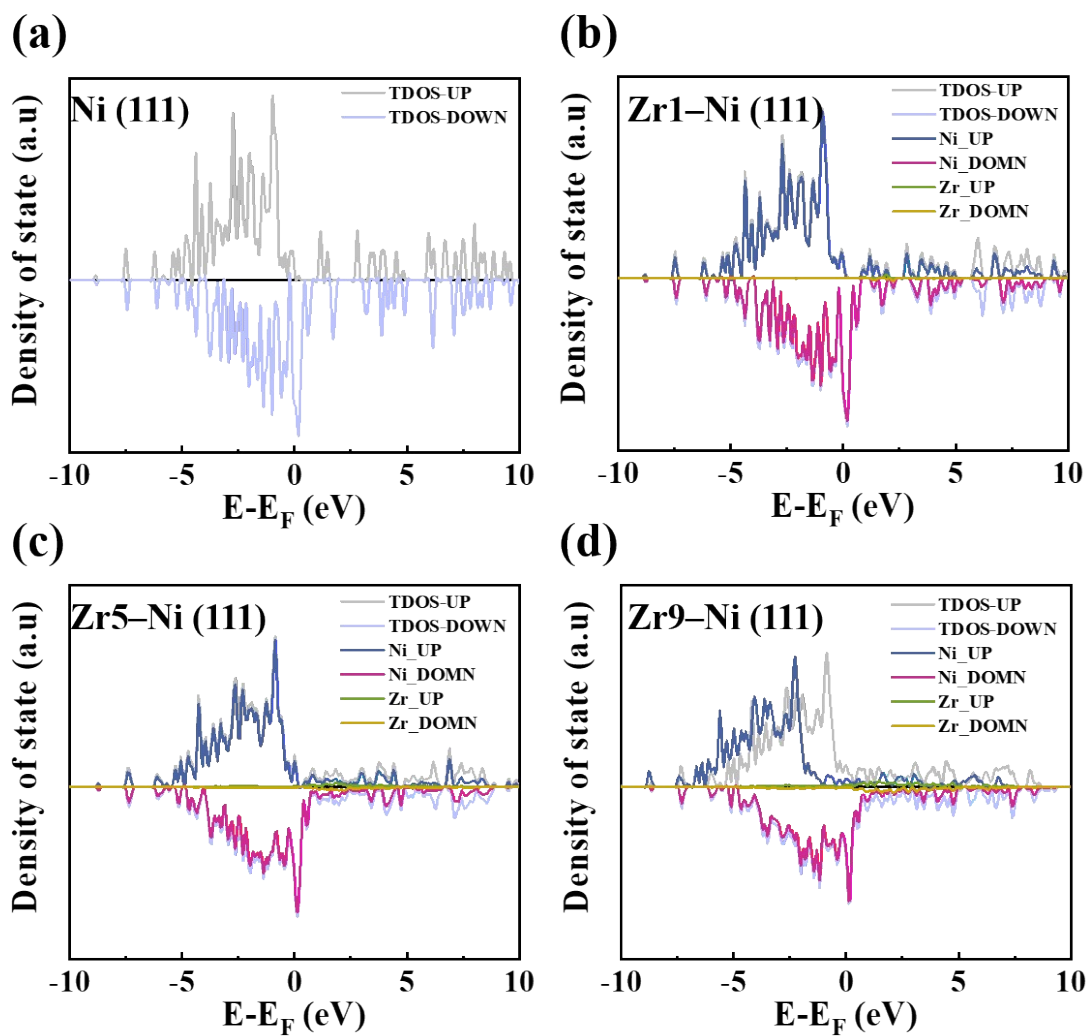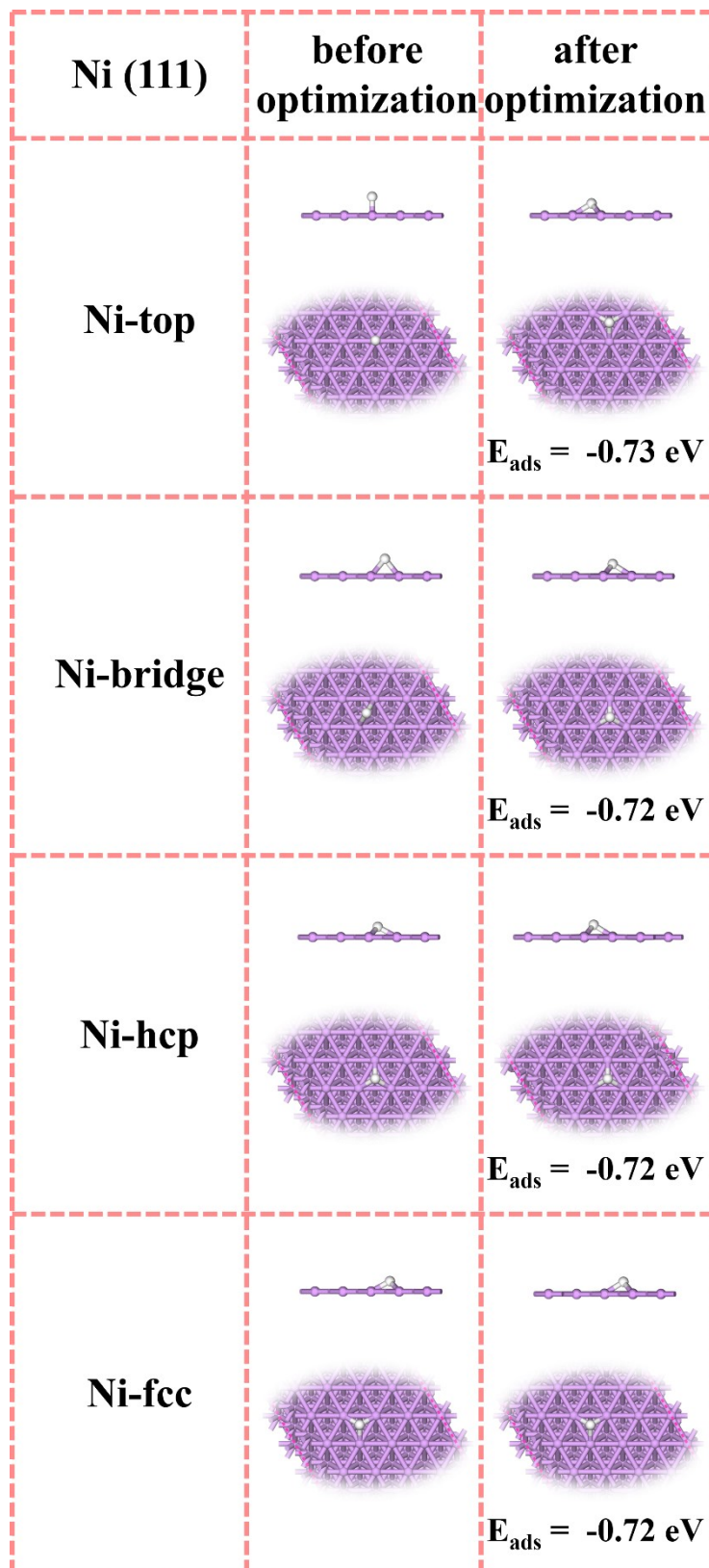
Fig. S2. The optimized possible catalyst's structure of (a1-a3) Zr5–Ni (111) surface and (b1-b5) Zr9–Ni (111) surface.
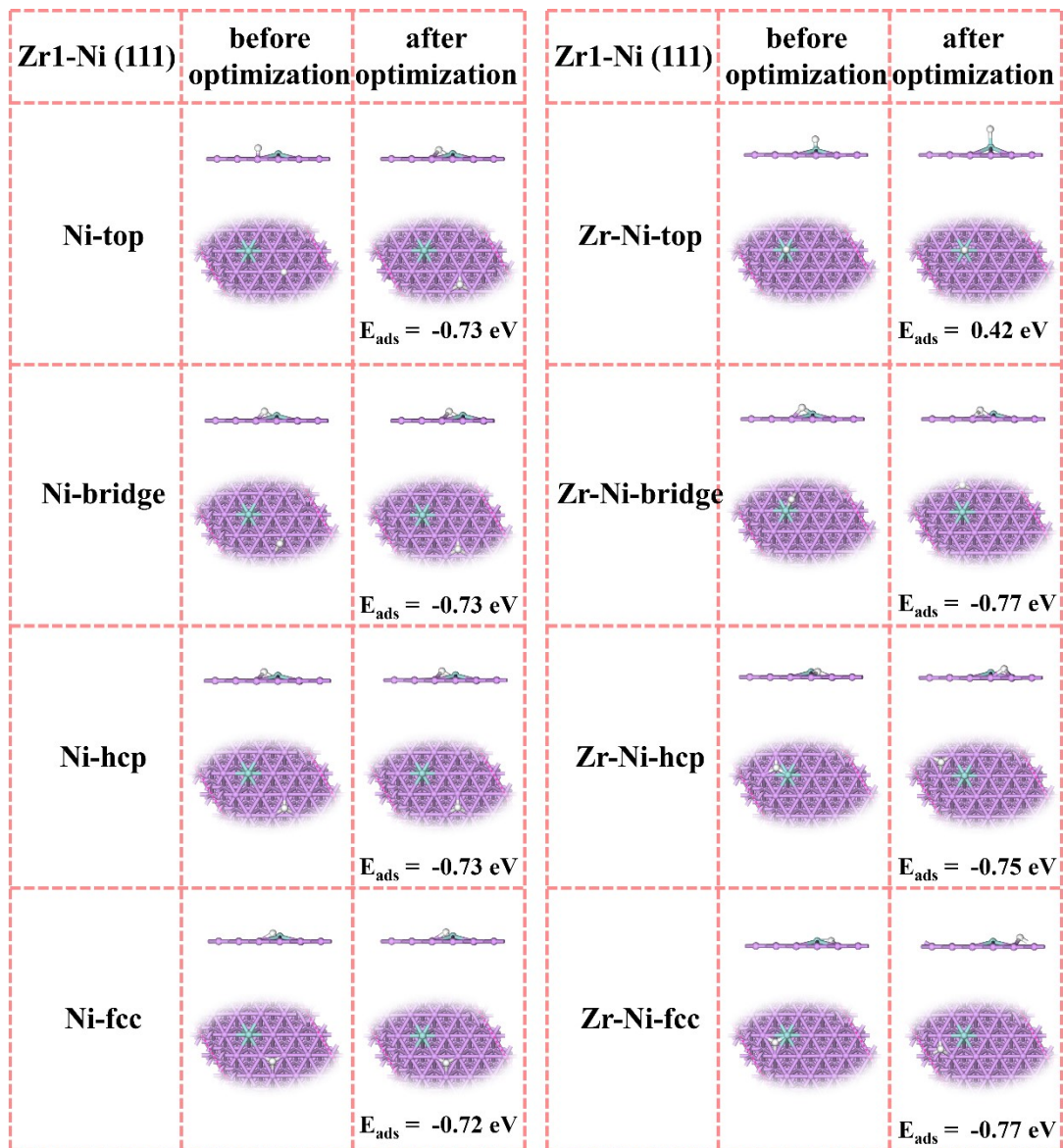
Fig. S3. Calculated Bader charge of (a) Zr1-Ni (111) (b) Zr5-Ni (111) and (c) Zr9-Ni (111) catalyst surface. Blue and red represent the electron accumulation and depletion region, respectively.

Fig. S4. Density of state (DOS) of Ni (111) (a), Zr1–Ni (111) (b), Zr5–Ni (111) (c) and Zr9–Ni (111) (d).

Ni (111)	before optimization	after optimization
Ni-top		$E_{ads} = -0.73$ eV
Ni-bridge		$E_{ads} = -0.72$ eV
Ni-hcp		$E_{ads} = -0.72$ eV
Ni-fcc		$E_{ads} = -0.72$ eV

Fig. S5. The side and top perspectives of the most stable adsorption energies and binding sites of the H atom on (a) Ni (111) surface.

Zr1-Ni (111)	before optimization	after optimization	Zr1-Ni (111)	before optimization	after optimization
Ni-top		$E_{ads} = -0.73$ eV	Zr-Ni-top		$E_{ads} = 0.42$ eV
Ni-bridge		$E_{ads} = -0.73$ eV	Zr-Ni-bridge		$E_{ads} = -0.77$ eV
Ni-hcp		$E_{ads} = -0.73$ eV	Zr-Ni-hcp		$E_{ads} = -0.75$ eV
Ni-fcc		$E_{ads} = -0.72$ eV	Zr-Ni-fcc		$E_{ads} = -0.77$ eV

Fig. S6. The side and top perspectives of the most stable adsorption energies and binding sites of the H atom on (a) Zr1-Ni (111) surface.

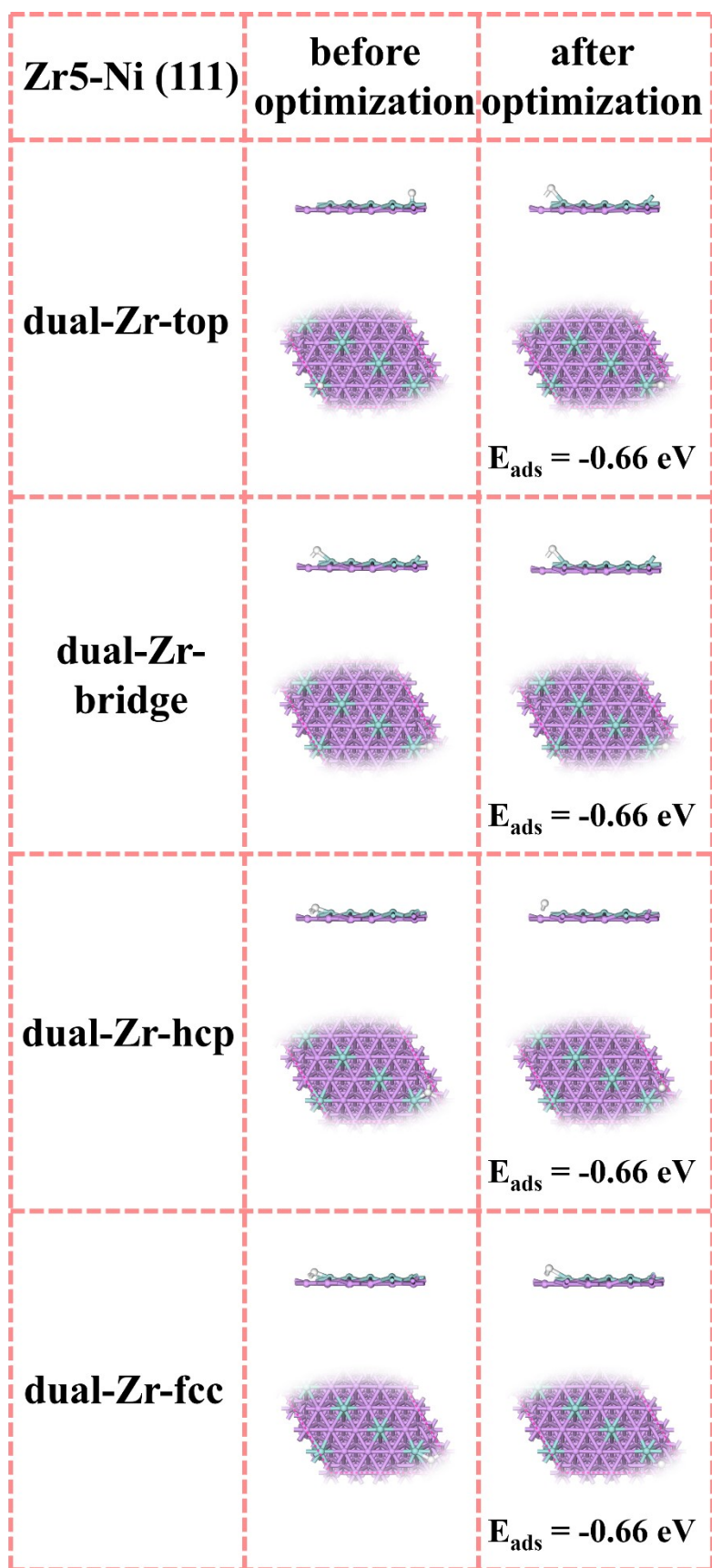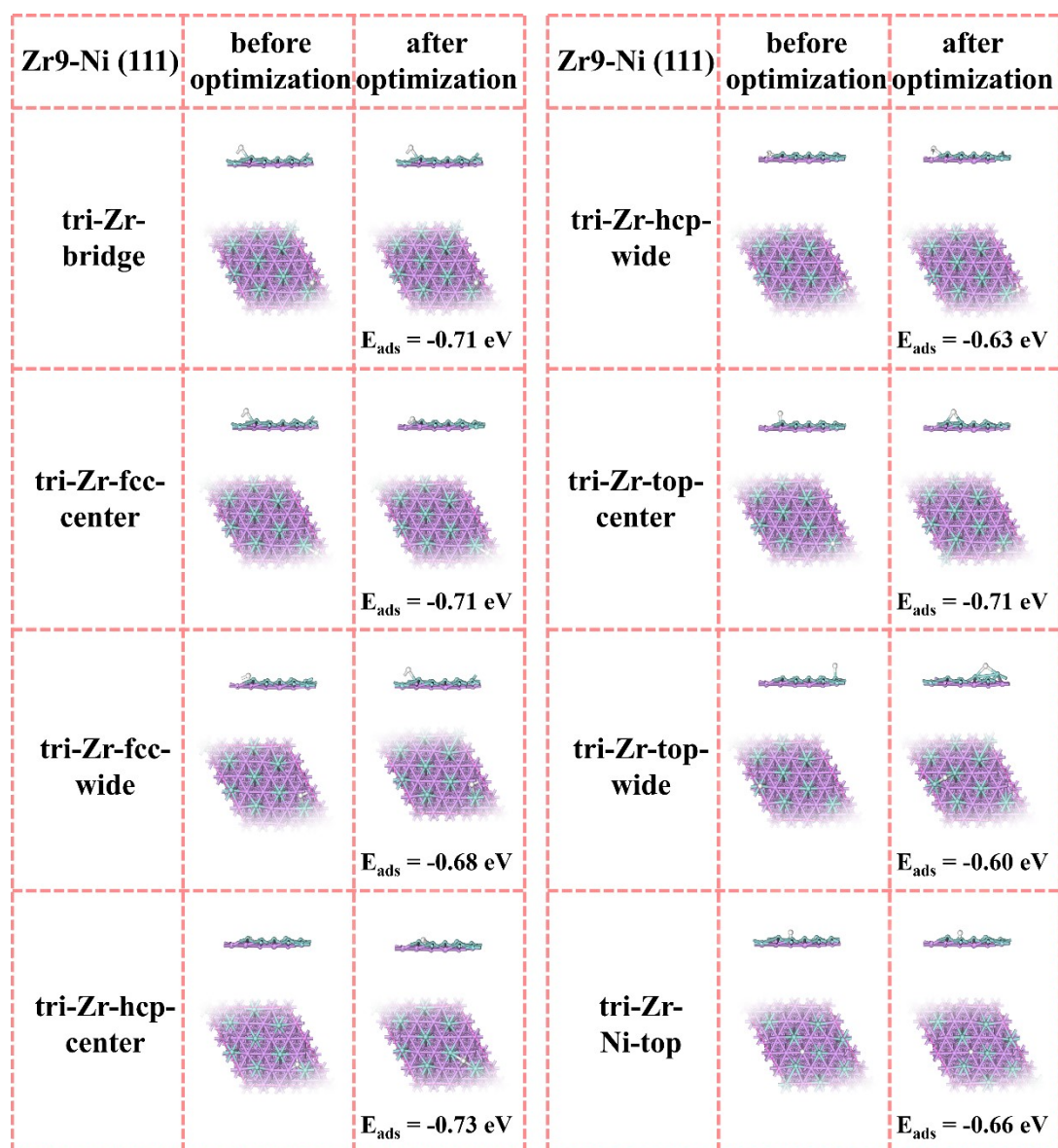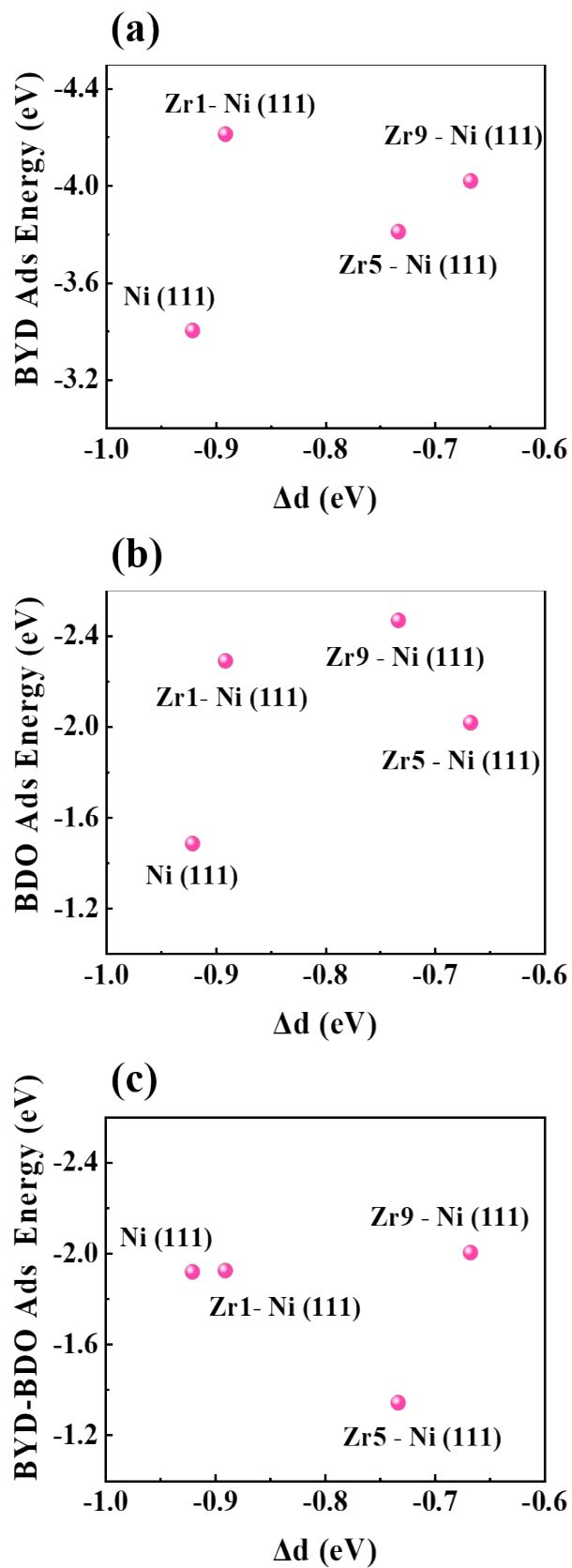| Zr5-Ni (111)	before optimization	after optimization
dual-Zr-top		E_{ads} = -0.66 eV
dual-Zr-bridge		E_{ads} = -0.66 eV
dual-Zr-hcp		E_{ads} = -0.66 eV
dual-Zr-fcc		E_{ads} = -0.66 eV

Fig. S7. The side and top perspectives of the most stable adsorption energies and binding sites of the H atom on Zr5-Ni (111) surface.

Zr9-Ni (111)	before optimization	after optimization	Zr9-Ni (111)	before optimization	after optimization
tri-Zr-bridge		$E_{ads} = -0.71$ eV	tri-Zr-hcp-wide		$E_{ads} = -0.63$ eV
tri-Zr-fcc-center		$E_{ads} = -0.71$ eV	tri-Zr-top-center		$E_{ads} = -0.71$ eV
tri-Zr-fcc-wide		$E_{ads} = -0.68$ eV	tri-Zr-top-wide		$E_{ads} = -0.60$ eV
tri-Zr-hcp-center		$E_{ads} = -0.73$ eV	tri-Zr-Ni-top		$E_{ads} = -0.66$ eV

Fig. S8. The side and top perspectives of the most stable adsorption energies and binding sites of the H atom on Zr9-Ni (111) surface.

Fig. S9. Correlation between the (a-c) Δd of Zrx-Ni (111) surface and different intermediates Ads energy (adsorption energy).
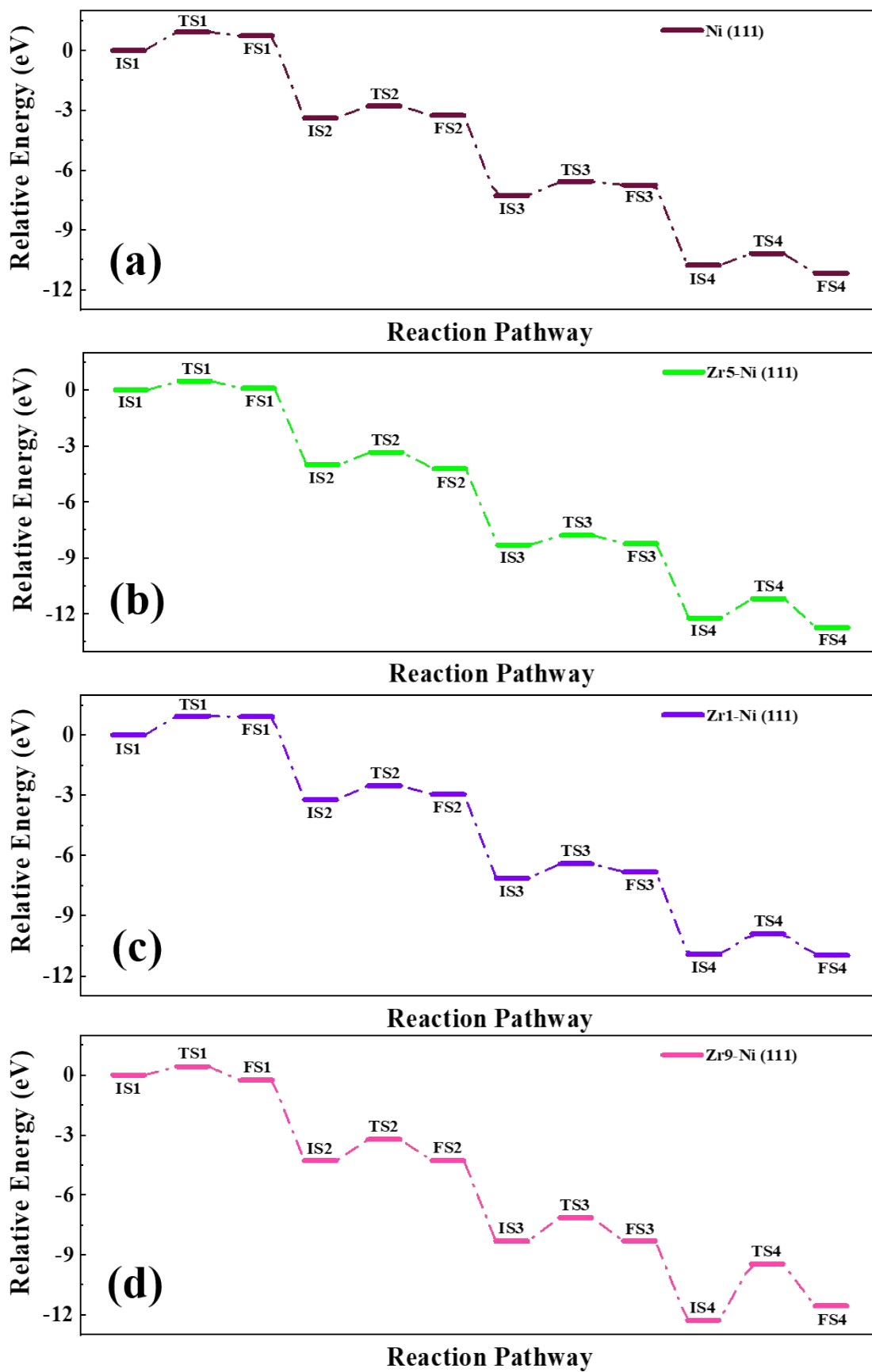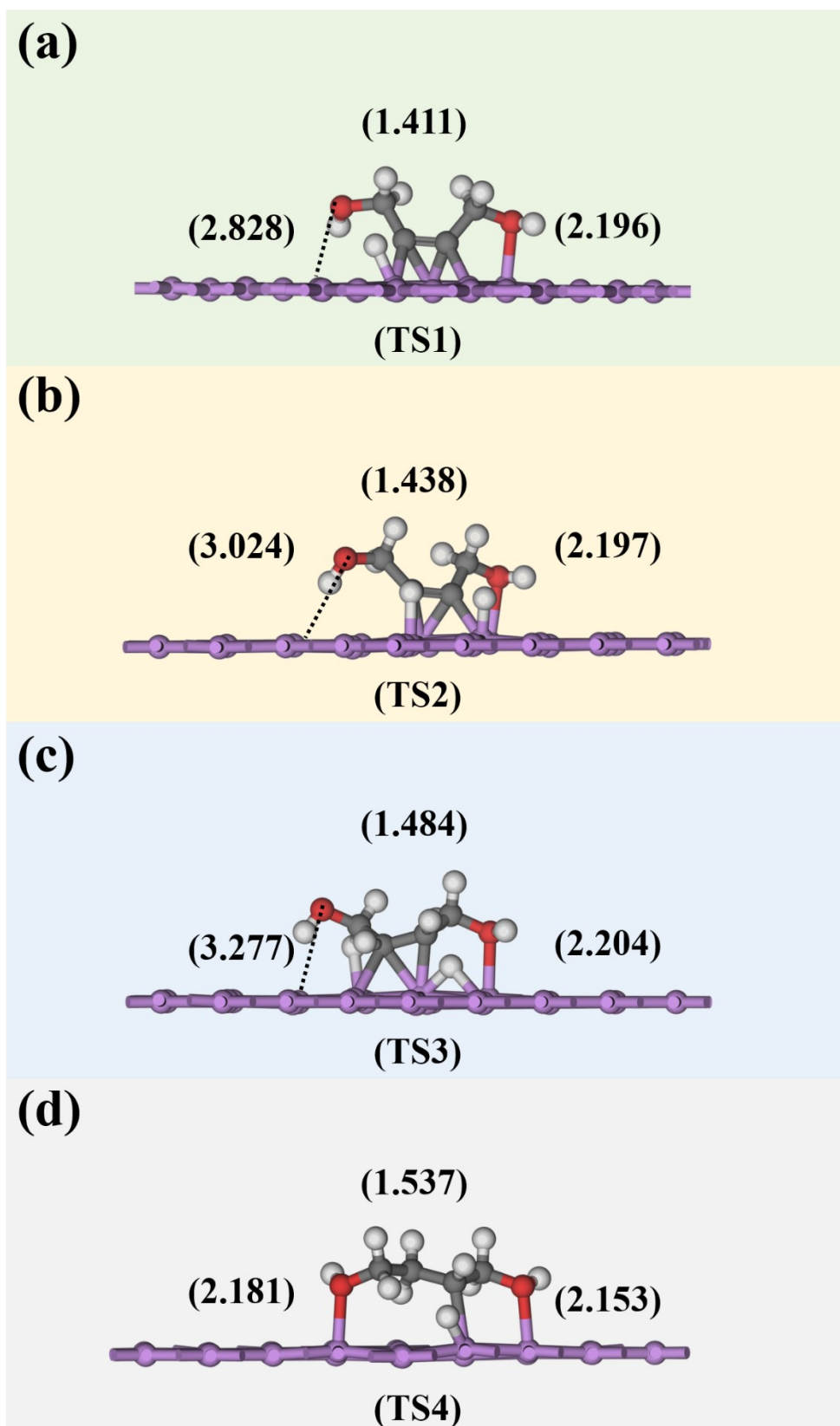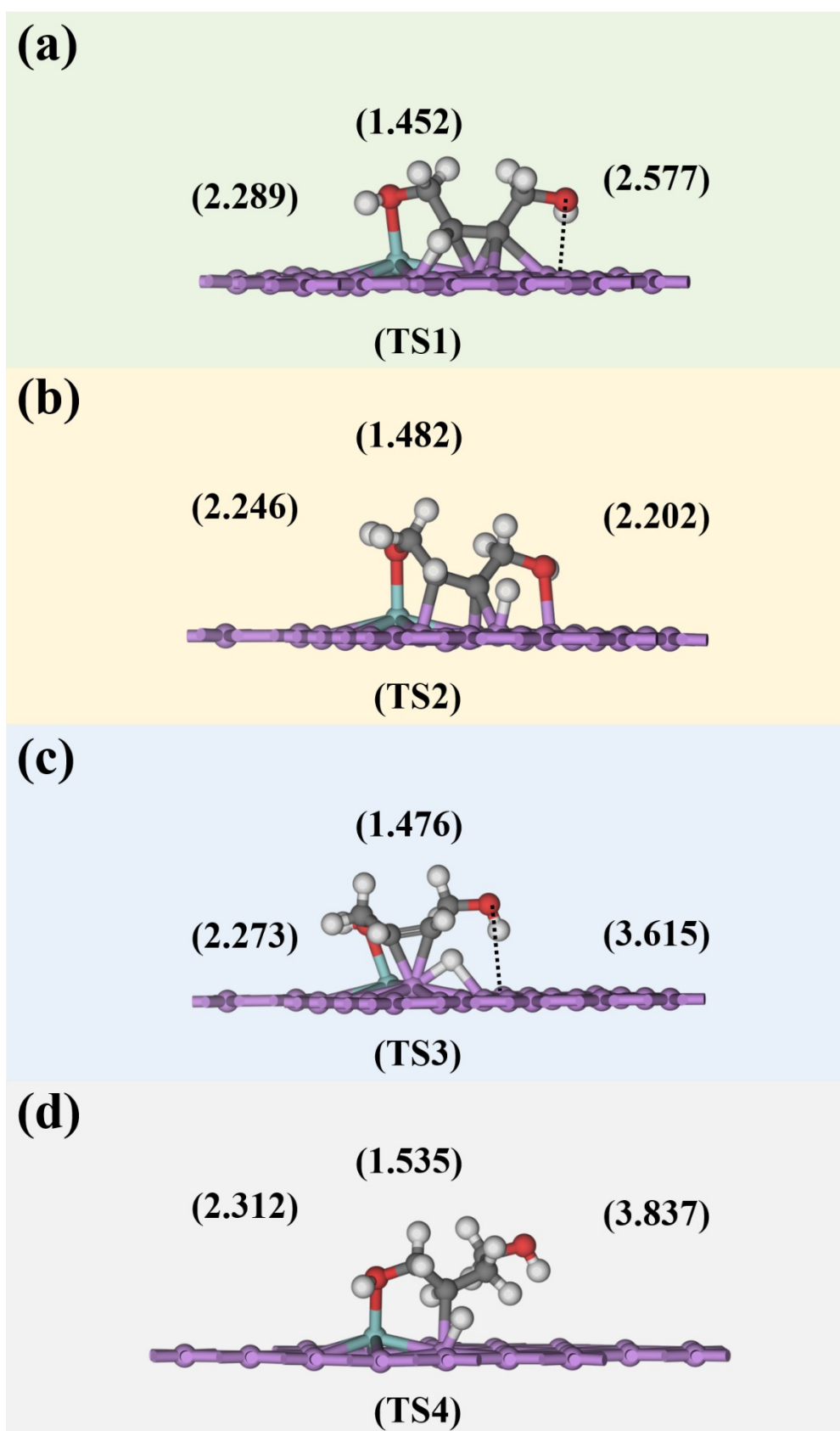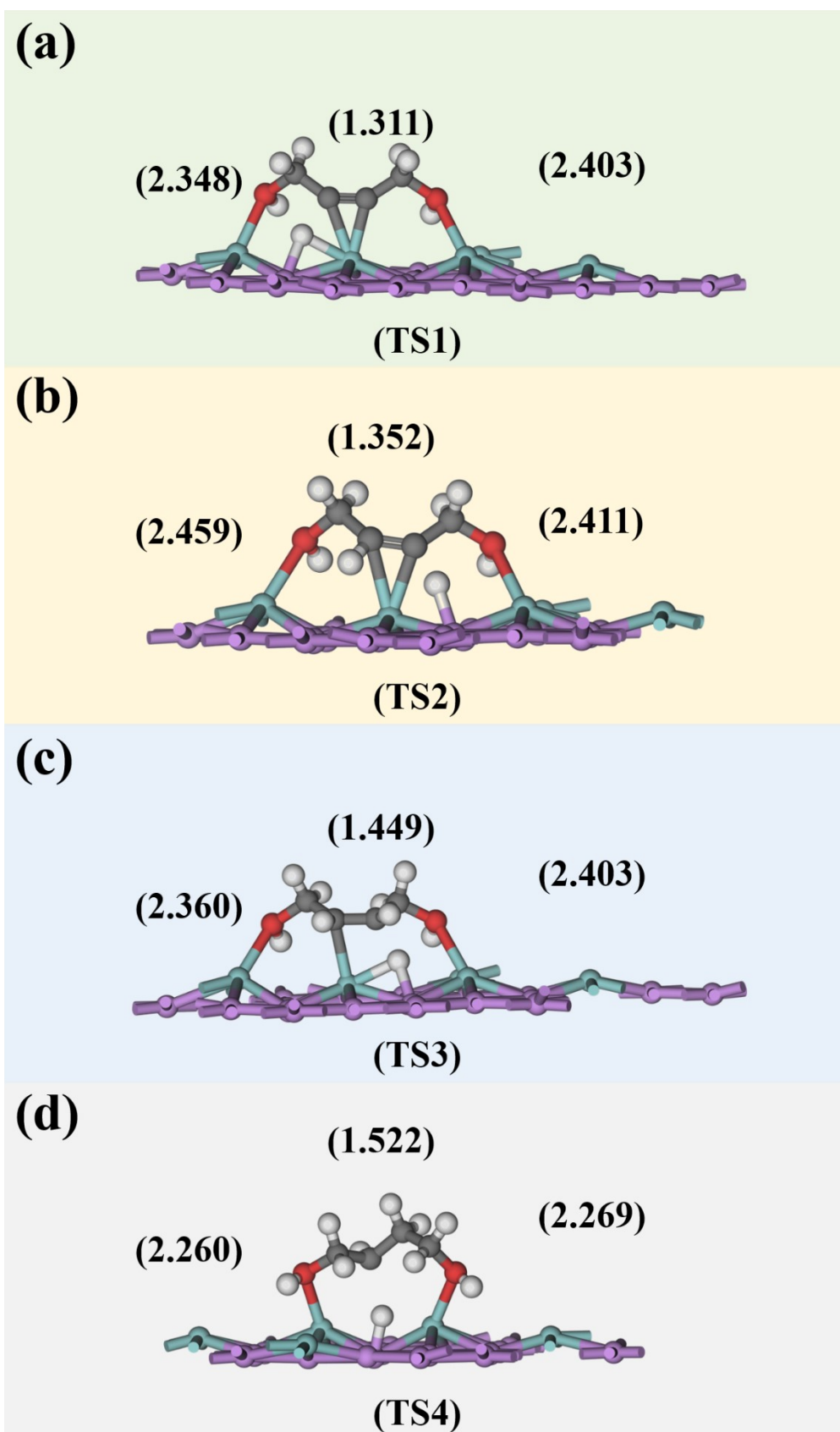
Fig. S10. Illustration of the whole energy diagram depicting the BYD hydrogenation process step on different catalysts.
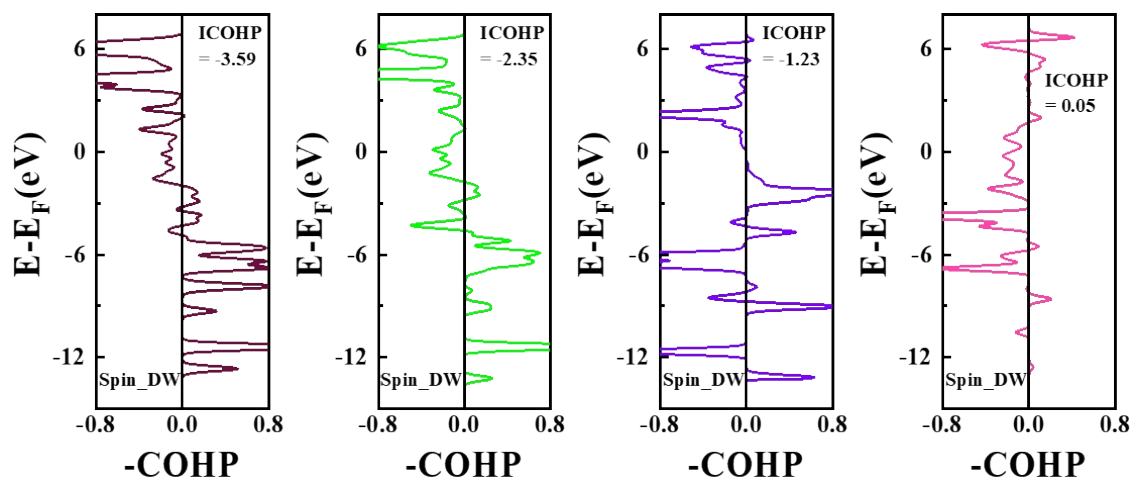
Fig. S11. Geometries of the transition states over the Ni (111). The numbers represent C-C triple bond and Zr-O bond lengths; bond lengths are in Å.
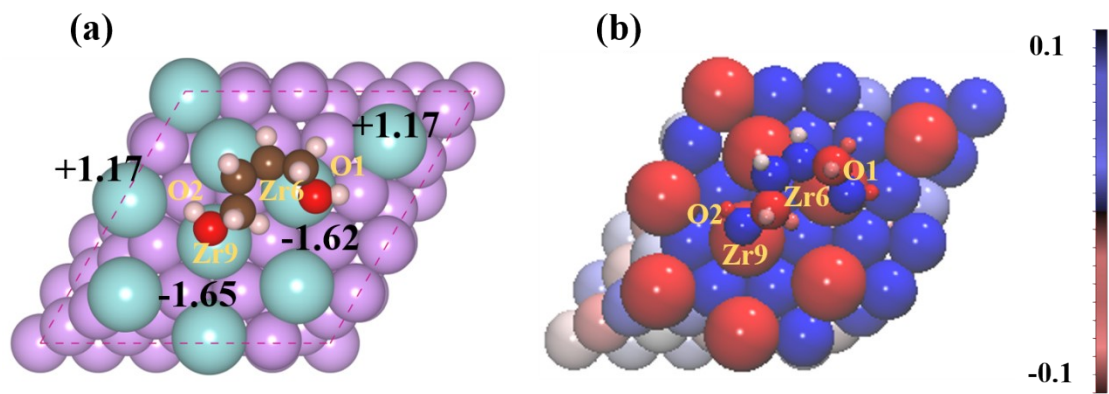
Fig. S12. Geometries of the transition states over the Zr1-Ni (111). The numbers represent C-C triple bond and Zr-O bond lengths; bond lengths are in Å.
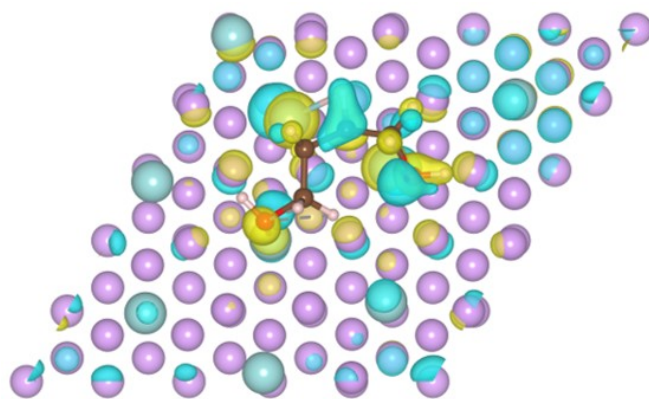
Fig. S13. Geometries of the transition states over the Zr5Ni (111). The numbers represent C-C triple bond and Zr-O bond lengths; bond lengths are in Å.

Fig. S14. The spin-down ICOHPs of C=C in cis-BED adsorbed on (a1) Ni (111), (b1) Zr1-Ni (111), (c1) Zr5-Ni (111), and (d1) Zr9-Ni (111). (a2-d2) is the PDOS of the absorbed cis-BED in Ni (111) or heterogeneous system.

Fig. S15. Calculated Bader charge of cis-BED adsorption on Zr9-Ni (111) catalyst surface. Blue and red represent the electron accumulation and depletion region, respectively.

Fig. S16. Charge density difference for cis-BED adsorption on Zr9-Ni (111). Cyan and yellow mean electron depletion and accumulation, respectively. The value of the isosurface is 0.1 eBohr^{-3}.

Table S1. Energy of Optimized structure of doping system.

Structure	Energy (eV)
Fig.1b	**-543.24167**
Fig.S1a1	-557.66932
Fig.S1a2	-560.46103
Figure1c	**-561.75564**
Fig.S1a3	-559.34194
Fig.S1b1	-571.62888
Fig.S1b2	-572.27950
Fig.S1b3	-575.61713
Fig.S1b4	-575.46736
Fig.S1b5	-576.97849
Figure1d	**-577.54820**

Table S2. The d-bands center of different site. The unit is eV.

	Ni (111)	Zr1-Ni (111)	Zr5-Ni (111)	Zr9-Ni (111)
α-spin d-bandcenter	-1.794	-1.774	-1.742	-1.778
β-spin d-band center	-0.873	-0.883	-1.009	-1.111
Total d-band center	-2.667	-2.657	-2.751	-2.889
Δd	-0.921	-0.891	-0.773	-0.667

References

1. G. Kresse and J. Furthmüller, *Comput. Mater. Sci.*, 1996, **6**, 15-50.
2. G. Kresse and J. Furthmüller, *Phys. Rev. B*, 1996, **54**, 11169-11186.
3. P. E. Blöchl, *Phys. Rev. B*, 1994, **50**, 17953-17979.
4. G. Kresse and D. Joubert, *Phys. Rev. B*, 1999, **59**, 1758-1775.
5. J. P. Perdew, K. Burke and M. Ernzerhof, *Phys. Rev. Lett.*, 1996, **77**, 3865-3868.
6. H. J. Monkhorst and J. D. Pack, *Phys. Rev. B*, 1976, **13**, 5188-5192.
7. S. Grimme, J. Antony, S. Ehrlich and H. Krieg, *J. Chem. Phys.*, 2010, **132**, 154104.
8. R. Nelson, C. Ertural, J. George, V. L. Deringer, G. Hautier and R. Dronskowski, *J. Comput. Chem.*, 2020, **41**, 1931-1940.
9. G. Henkelman, B. P. Uberuaga and H. Jónsson, *J. Chem. Phys.*, 2000, **113**, 9901-9904.
10. G. Henkelman and H. Jónsson, *J. Chem. Phys.*, 1999, **111**, 7010-7022.
11. A. Heyden, A. T. Bell and F. J. Keil, *J. Chem. Phys.*, 2005, **123**, 224101.